Korean J. Chem. Eng., 32(8), 1667-1677 (2015)
DOI: 10.1007/s11814-014-0352-4

pISSN: 0256-1115
eISSN: 1975-7220

Abatement of Cr(VI) and As(III) by MnO_2 loaded MCM-41 in wastewater treatment

Yunhai Wu*, Shengxin Yang, Meili Zhang**, Ayinigaer Aierken**, and Yunying Wu***,†**

*Key Laboratory of Integrated Regulation and Resources Development of Shallow Lakes, Ministry of Education, Hohai University, Xikang Road #1, Nanjing 210098, China
**College of Environment, Hohai University, Xikang Road #1, Nanjing 210098, China
***Department of Chemistry, Hanshan Normal University, Chaozhou, Guangdong Province, China
(*Received 24 September 2014 • accepted 28 November 2014*)

Abstract−Manganese dioxide (MnO_2) loaded MCM-41 (MnO_2/MCM-41) was used as adsorbent to remove Cr(VI) and As(III) from aqueous solution. The adsorbent was synthesized and characterized. Effect of pH on the removal of Cr(VI) and As(III) was investigated. The desired pH of aqueous solution was 2 for the removal of Cr(VI) and 4 for the removal of As(III). Besides, the adsorption of As(III) and Cr(VI) can be well described by Langmuir and Freundlich isotherm models, respectively. The kinetic data can be successfully depicted by pseudo-second-order model. Moreover, external and intra-particle diffusion were found to be rate-controlling steps of the adsorption process. Thermodynamic analysis suggested that the adsorption process was spontaneous and endothermic. In a binary system, the presence of Cr(VI) and As(III) slightly reduced the removal efficiency of each other. The desorption study showed 0.1 mol/L NaOH liquor held good desorption ability for metal loaded MnO_2/MCM-41.

Keywords: MnO_2/MCM-41, Adsorption, Isotherm, Kinetic, Thermodynamic, Binary System

INTRODUCTION

More and more attention is being focused toward the pollution caused by existence of heavy metals, such as Cr(VI) and As(III) in ecosystem [1]. These pollutants accumulate in living tissues throughout food chain and cause serious health problems [2]. Chromium is one of the most highly toxic heavy metal pollutants in wastewater. In aqueous solution, chromium mainly exists in two states: Cr(III) and Cr(VI). Cr(VI) is extremely more hazardous than Cr(III) for its toxicity, mobility and hard degradation [3]. The maximum acceptable concentration of Cr(VI) in wastewater has been set as 50 μg/L by the US Environmental Protection Agency [4]. Arsenic has also been recognized worldwide as one of the most harmful pollutants [5]. It has been reported that drinking water contaminated by arsenic with concentration equal to or greater than 50 ppb increases the risks of lung, bladder cancer and arsenic-associated skin lesions [6,7]. Therefore, the World Health Organization (WHO) has set concentration limits for drinking water at 10 ppb As [8].

In terms of the removal of Cr(VI) and As(III), a variety of methods have been used: adsorption, complexation, chemical precipitation, solvent extraction, reverse osmosis, ion exchange, filtration and membrane processes [3,9,10]. Among them, adsorption is one of the most effective and attractive because of easy operation, high efficiency over a broad concentration range and low secondary pollution with the suitable regeneration operation [11]. The previous used adsorbents, which have been explored for their capability in the removal of heavy metal ions from aqueous solution, include activated carbons from different sources [12,13], biomass (*mycobacterium* [14], *chitosan* [15] and *peat moss* [16]), minerals (dolomite [17], zeolites [17] and kaolinite-based clay [18]) and synthetic polymers [19,20]. However, many of these have drawbacks such as limited selectivity, low equilibrium adsorption capacity and long equilibrium time. Silica-based adsorbents have attracted considerable attention due to their large surface area, regular pore structure, easily modified surface properties and controlled pore diameter [21]. More importantly, mesoporous silicas can be modified to alter their properties and achieve particular purposes. Among mesoporous silicas, MCM-41 shows high removal rate and selectivity, short equilibrium time and good mechanical stability in the adsorption of heavy metal ions from aqueous solution [22,23]. In the literature, amine-functionalized MCM-41 [24], TiO_2 grafted MCM-41 [25] have been used to eliminate heavy metal from wastewater. In addition, Mn, MnO_2 or manganese mineral as catalyst or adsorbent have been studied for their performance [26,27] as well as manganese oxide coated media, such as MnO_2-modified expanded graphite nano-composites [28], MnO_2/carbon nanotubes [29], MnO_2-loaded resin [30] and so on. Thereby, for the purpose of improving performance of MCM-41 in heavy metal removal, MnO_2 loaded MCM-41 was used to deal with heavy metals in this work.

In the present work, MnO_2 was first loaded onto MCM-41 to develop an adsorbent, and this composite was used to remove Cr(VI) and As(III) from single and binary aqueous solution. Effect of pH was studied and adsorption equilibrium data, kinetic and thermodynamic parameters were calculated to determine the adsorption mechanism. The purpose of this study was to explore the adsorption process and availability of MnO_2/MCM-41 to absorb Cr(VI)

†To whom correspondence should be addressed.
E-mail: ysxhohai@sina.cn

and As(III) from aqueous solution.

MATERIALS AND METHODS

1. Materials

Stock solutions of Cr(VI) (100 mg/L) and As(III) (1,000 mg/L) were prepared by dissolving 0.2829 g dried potassium dichromate ($K_2Cr_2O_7$) (Guangfu Fine Chemical, Tianjin, China) and 1.7333 g dried sodium arsenite ($NaAsO_2$) (Third Chemical Reagent Factory, Beijing, China) in 1,000 mL distilled water (SAGA Instrument Co., Ltd., Shanghai, China), respectively. Experimental solutions of different concentrations were obtained by diluting stock solution with suitable volume of distilled water. pH of the solution was adjusted to required values using 0.1 M HCl (Pilot Chemical Co., Shanghai, China) or NaOH (First Chemical Reagent Factory, Nanjing, China). All reagents used were of analytical-reagent grade, and distilled water was used to prepare all the solutions.

2. Adsorbent Synthesis

MCM-41 was prepared from alkaline synthesis solution according to the method of Jana et al. [31]. And MnO_2/MCM-41 was synthesized by a redox-precipitation method as follows: first, a mixture of 5.0 g MCM-41 and 50 mL manganese chloride (0.6 mol/L) (Xilong Chemical Co., Ltd., Guangdong, China) was agitated using a magnetic stirrer at room temperature for 5 min. Then, 5.27 g potassium permanganate (Jiuyi Chemical Reagent Co., Ltd., Shanghai, China) was added into the above solution mixture and stirred for 5 h. The reaction can be expressed by the equation follows:

$$3Mn^{2+}+2MnO_4^-+2H_2O=5MnO_2\downarrow+4H^+ \quad (1)$$

Finally, the mixture was filtered, washed with distilled water for several times and dried at room temperature for 48 h.

3. Physic-chemical Characterization

X-ray diffraction (XRD) patterns of the adsorbent were recorded on an X-ray diffractometer (ARL Corporation, Switzerland) using Ni filter CuKα (40 kV and 200 mA) in the range of 1° to 8° and 10° to 80° (2θ). An X-ray fluorescence (XRF) analyzer (Thermo Fisher Scientific Corporation, US) was used to judge the composition of MnO_2/MCM-41 before and after adsorption. The surface morphology of the samples was investigated by a scanning electron microscope (SEM) (S4800, Carl Zeiss AG, Germany) and the images were taken at 10.0 kV.

4. Adsorption Studies

Batch adsorption experiments were investigated by adding a predetermined amount of MnO_2/MCM-41 into 250 mL glass conical flasks containing 20 mL solution with known Cr(VI) and As(III) concentration. Then these flasks were placed in a water bath shaker (Jintan Ronghua Instrument Manufacture Co., Ltd., Jiangsu, China) at 130 rpm for 5 h under temperature of 298±1 K. Effect of pH on the sorption capacity of MnO_2/MCM-41 was evaluated by adjusting pH in the range of 2-9. For isotherm studies, experiments were conducted at three different temperatures: 298, 313 and 328 K. Adsorption kinetic studies were carried out at pH 2, 298 K, and the samples were withdrawn at predetermined time intervals. Concentrations of Cr(VI) and As(III) used in the kinetic studies were 10, 20 and 30 mg/L and 2, 5 and 8 mg/L, respectively. For binary component adsorption experiments, the experiment solution was obtained by mixing identical volume of Cr(VI) (20 mg/L) and As(III) (5 mg/L). After adsorption, the adsorbent was separated by centrifugation at 4,000 rpm for 10 min. Residual Cr(VI) and As(III) concentration in the supernatant was determined by a UV-spectrophotometer (Rayleigh UV1201, Beijing, China) at wavelength of 540 nm and 510 nm, respectively. The removal (%) of Cr(VI) and As(III) was calculated for each run using the following expression:

$$\text{Removal}=\frac{C_0-C_e}{C_0}\times 100\% \quad (2)$$

Adsorption capacity (mg/g) of MnO_2/MCM-41 for each concentration of Cr(VI) and As(III) ions at equilibrium was determined as follows:

$$q_e=\frac{(C_0-C_e)V}{M} \quad (3)$$

All these experiments were conducted in duplicate and average of the two values was used. The maximum difference between the two values was less than 3% of the value.

5. Regeneration of Adsorbent

After adsorption process, the adsorbent was collected and dried. Then, the desorption studies were performed by agitating 0.1 g of metal ions loaded adsorbent with 100 mL of 0.1 mol/L NaOH (First Chemical Reagent Factory), HCl (Pilot Chemical Co.), $NaNO_3$, Na_2CO_3 and Na_3PO_4 (Sinopharm Chemical Reagent Co., Ltd.), respectively, at 303 K. Five hours later, the mixture was filtered and desorption solution was determined to calculate desorption efficiency by equation follows:

$$\beta=\frac{C_2\times V_2}{(C_0-C_e)\times V_1}\times 100\% \quad (4)$$

Before being reused in the adsorption-desorption cycle, the collected adsorbent was washed with excess distilled water. And then, it was reused in the adsorption-desorption cycle for six times to evaluate its reusability.

RESULTS AND DISCUSSION

1. Characterization of MnO_2/MCM-41

Small angle XRD patterns of MCM-41 and MnO_2/MCM-41 are shown in Fig. 1(A); the patterns presented strong peaks in low angle 1-3° (2θ), corresponding to the diffraction of (100) plane. These diffraction peaks were attributed to reflection and characteristic of mesostructure of MCM-41 [32]. Therefore, it can be confirmed that the mesoporosity and integrated framework of ordered MCM-41 was preserved after MnO_2 loaded. However, the diffraction peak (100) plane of MnO_2/MCM-41 became weaker and the diffraction peak (110) plane disappeared when compared with that of MCM-41, which may result from the loading of MnO_2. After MnO_2 was loaded on MCM-41, the agglomerate of MnO_2 particles and the interaction of MCM-41 framework led to increase of lattice defect and the reduction of tunnel size [33]. Fig. 1(B) illustrates the wide-angle XRD pattern of MCM-41 before and after MnO_2 loading. Compared with MCM-41, MnO_2/MCM-41 exhibited two peaks at 37.5° and 66.3°, which were attributed to the existence of MnO_2 crystal and amorphous MnO_2 [34,35]. Thus, it can be concluded

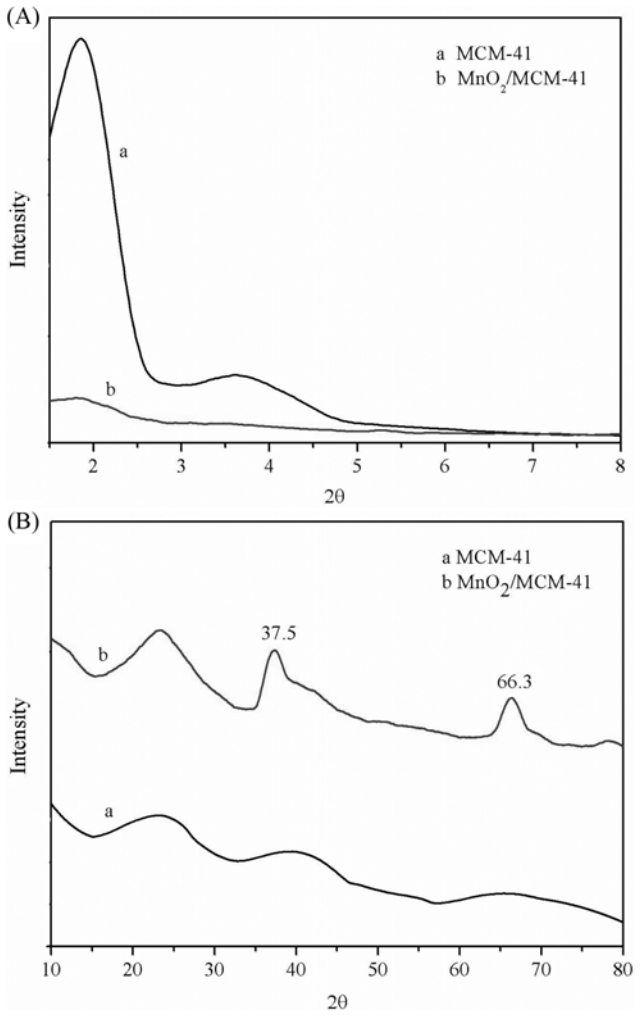

Fig. 1. (A) Small angle XRD pattern of MCM-41 and MnO_2/MCM-41, (B) wide angle XRD pattern of MCM-41 and MnO_2/MCM-41.

that MnO_2 was successfully loaded on MCM-41. Moreover, the loaded MnO_2 was mainly MnO_2 crystal and the peaks at 37.5° and 66.3° can be ascribed to the crystal planes of (111) and (020) in the birnessite (γ-MnO_2, Joint Committee on Power Diffraction Standards (JCPDS) 42-1317), respectively [34,36,37], namely, there was little amorphous MnO_2.

The chemical composition of MnO_2/MCM-41 before and after adsorption was analyzed through XRF. And the scanning data are presented in Table 1. Note that the primary constituents MnO, SiO_2 and Al_2O_3 were recorded, which came from the synthesis process of MnO_2/MCM-41. While the existence of CrO_3 and As_2O_5 was attributed to the Cr(VI) and As(III) solution, respectively, indicating the metal ions were adsorbed on MnO_2/MCM-41.

Table 1. The XRF scanning data of MnO_2/MCM-41 before and after adsorption

Compound	Composition (m/m%)		
	MnO_2/MCM-41	Cr(VI) loaded MnO_2/MCM-41	As(III) loaded MnO_2/MCM-41
MnO	46.27	44.19	46.07
SiO_2	46.75	51.44	48.37
Al_2O_3	1.78	1.82	0.11
CrO_3	0	0.0463	0
As_2O_5	0	0	0.0045

SEM micrographs, presented in Fig. 2, show the surface morphology of MCM-41, MnO_2/MCM-41 and metal loaded MnO_2/MCM-41. Comparing Fig. 2(a) with Fig. 2(b), more brilliant particles on the surface of MCM-41 can be clearly detected, which may be caused by the loading of MnO_2. Kureshy et al. [38] showed the SEM micrographs of MCM-41 and Mn(III) incorporated MCM-41, on whose surface small agglomerates appeared as well. Fig. 2(c) shows that crystal grain formed and accumulated on MnO_2/MCM-41 when As(III) ions reacted with the adsorbent. Thus, it maybe deduced that partial As(III) was adsorbed on the adsorbent surface. Besides, lumpy material can be observed from the image (Fig. 2(d)) of Cr(VI) loaded MnO_2/MCM-41, which was caused by adsorption of Cr(VI). Combining SEM with the XRD and XRF analysis, these results strongly proved that MnO_2 was successfully fixed with MCM-41, while Cr(VI) and As(III) were effectively adsorbed by MnO_2/MCM-41.

2. Comparison of Removal Efficiency before and after MnO_2 Loaded

MnO_2/MCM-41 exhibited high affinity for Cr(VI) and As(III). As can be seen from Fig. 3, there is a noticeable increase in the removal efficiency of Cr(VI) and As(III) by MnO_2/MCM-41 when compared with that of MnO_2 and MCM-41. For instance, the removal of Cr(VI) and As(III) by MnO_2/MCM-41 reached 75.32% and 85.78%, respectively, whereas for MnO_2 and MCM-41 the values were Cr(VI) (42.08%), As(III) (43.68%) and Cr(VI) (39.48%), As(III) (20.03%), respectively. These results indicated that MnO_2/MCM-41 had the potential to be used in the removal of Cr(VI) and As(III) from aqueous environment.

3. Adsorption Tests in Single System

3-1. Effect of pH

Initial pH of aqueous solution is an important controlling parameter in the adsorption process. Variation in pH affects not only the surface charge of the adsorbent but also the ionization and speciation of chromium and arsenic [39]. Fig. 4 presents the adsorption capacity of MnO_2/MCM-41 for Cr(VI) and As(III) against initial solution pH.

As can be seen from Fig. 4, the adsorption capacity for Cr(VI) was dramatically affected by solution pH. Moreover, it was also observed that, up to pH 9, an increase in pH resulted in decreasing Cr(VI) uptake. The maximum adsorption capacity (7.0 mg/g) occurred at pH 2.0. In aqueous solution, Cr(VI) exists mainly in five species including CrO_4^{2-}, $HCrO_4^-$, $Cr_2O_7^{2-}$, $HCr_2O_7^-$ and H_2CrO_4 depending on pH. The different species can be expressed by equilibrium reaction [40]:

$$H_2CrO_4 = H^+ + HCrO_4^-,\ K = 1.6\times10^{-1} \quad (5)$$

$$HCrO_4^- = H^+ + CrO_4^{2-},\ K = 3.2\times10^{-7} \quad (6)$$

$$2HCrO_4^- = H_2O + Cr_2O_7^{2-},\ K = 33.1 \quad (7)$$

$HCrO_4^-$ is the prevalent form of hexavalent chromium at low pH,

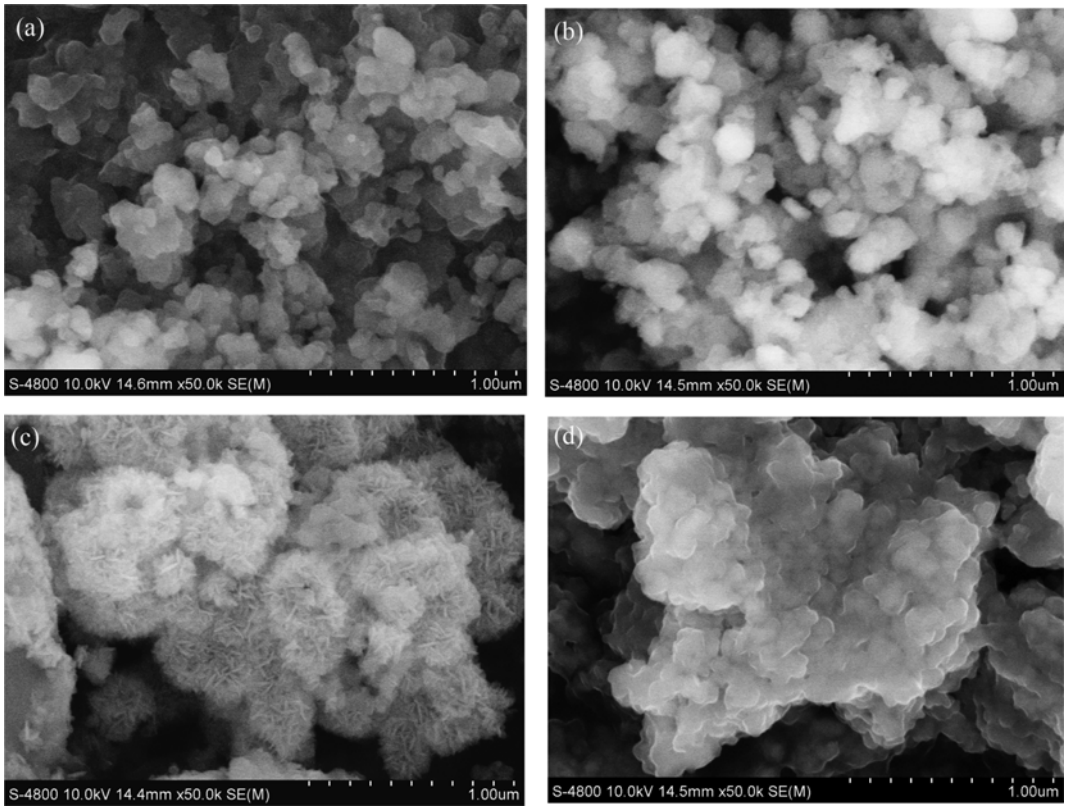

Fig. 2. SEM micrographs: MCM-41 (a), MnO_2/MCM-41 (b), As loaded MnO_2/MCM-41 (c), Cr loaded MnO_2/MCM-41 (d).

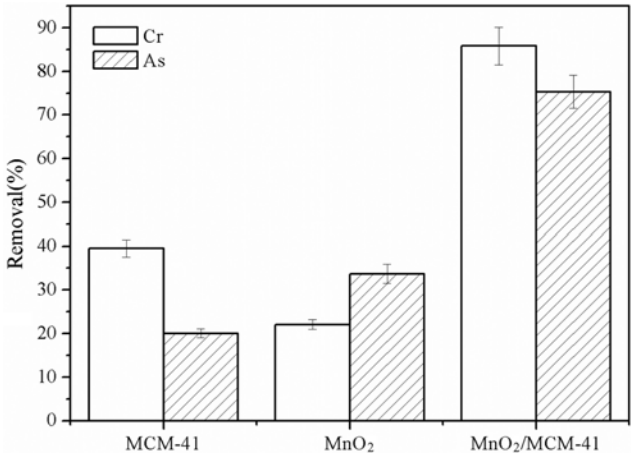

Fig. 3. Comparison of the removal of Cr(VI) and As(III) by MCM-41, MnO_2 and MnO_2/MCM-41 (initial concentration of Cr (VI) and As(III)-10 mg/L; adsorbent dosage of MCM-41, MnO_2 and MnO_2/MCM-41 –0.1 g, 0.1 g and 0.1 g; contact time-180 min).

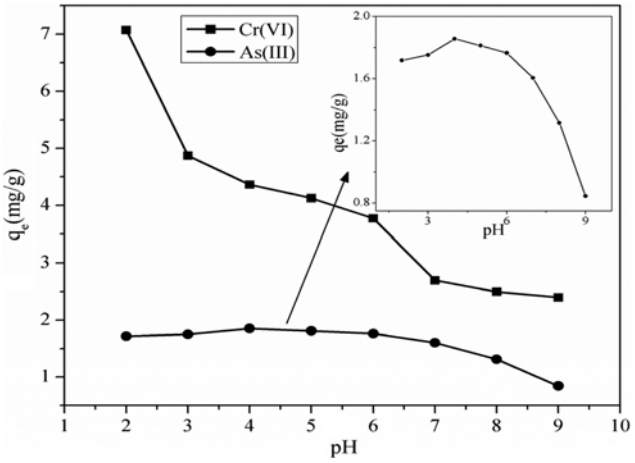

Fig. 4. Effect of pH on the adsorption of Cr(VI) and As(III) onto MnO_2/MCM-41 (initial concentration of Cr(VI)-20 mg/L, As(III)-5 mg/L; adsorbent dosage-0.5 g; contact time-300min; temperature-298 K).

which subsequently shifts to other forms: for example, CrO_4^{2-} and $Cr_2O_7^{2-}$ when the pH increases. Besides, at low pH, adsorbent surface would be protonated to a high extent under acidic condition; thus there existed strong attraction between the negatively charged Cr(VI) ions ($HCrO^-$) and positively charged sorbent surface [41], increasing the adsorption toward Cr(VI) ions. While, at higher pH, competition between OH^- and the bichromate anion (CrO_4^{2-} and $Cr_2O_7^{2-}$) for effective adsorption sites would lead to a reduction in the adsorption of Cr(VI) [42]. The surface of the adsorbent was negatively charged at higher pH, so repulsion between the anion of Cr(VI) (CrO_4^{2-} and $Cr_2O_7^{2-}$) and the adsorbent may also have contributed to the low adsorption capacity.

Fig. 4 also shows the effect of pH on adsorption capacity of MnO_2/MCM-41 toward As(III). At pH 2-4, an increase in pH led to increasing As(III) uptake. The biggest adsorption capacity was achieved

at pH 4. When pH value was larger than 4, the uptake decreased slowly with increasing pH up to 6. However, it decreased sharply when pH exceeded 6. In pH range of 2-4, $H_3AsO_3^0$ was present, van der Waals force between adsorbent surface and adsorbate stimulated the adsorption of As(III). While at about 4-6.9, $H_2AsO_3^-$ dominated; the adsorption capacity dropped owing to the charged repulsion force between anions and the negatively charged adsorbent. Because $HAsO_3^{2-}$ was dominant when pH was higher than 6, a stronger repulsion force led to a sharply decrease of the adsorption towards As(III) [10,43]. Aside from the impact of electronic attraction, the oxidant power of MnO_2 under acidic condition may also play a role in the adsorption of As(III) ($H_3AsO_3^0$ or $H_2AsO_3^-$). This is because As(III) ($H_3AsO_3^0$ or $H_2AsO_3^-$) could be oxidized into As(V) (H_3AsO_4), which is more easily to precipitate. The redox reaction may be expressed by the following equation [44]:

$$2MnO_2+H_3AsO_3+H_2O=2MnOOH^*+H_3AsO_4 \quad (8)$$

$$2MnOOH^*+H_3AsO_3+4H^+=2Mn^{2+}+H_3AsO_4+3H_2O \quad (9)$$

where $MnOOH^*$ represents a kind of chemical substance consisting of Mn(III), H^+ and H_2O.

3-2. Adsorption Isotherm

For purpose of optimizing the procedure, Langmuir, Freundlich and Dubinin-Radushkevich (D-R) isotherm models were used to model the experimental data and report good correlation. The Langmuir model assumes a monolayer adsorption and insists that there exists no interaction between the adsorbed molecules [45]:

$$q_e=\frac{q_m K_L C_e}{1+K_L C_e} \quad (10)$$

The Freundlich isotherm is usually used for assuming an uneven distribution of adsorption heat over the surface and non-ideal multilayer adsorption [46]:

$$q_e=K_F C_e^{1/n} \quad (11)$$

The D-R model is mainly used to evaluate adsorption energy [47] and describe sorption on both homogeneous and heterogeneous surfaces:

$$q_e=q_m \exp(-K\varepsilon^2) \quad (12)$$

$$\varepsilon=RT \ln\left(1+\frac{1}{C_e}\right) \quad (13)$$

$$E=\frac{1}{\sqrt{2K_{DR}}} \quad (14)$$

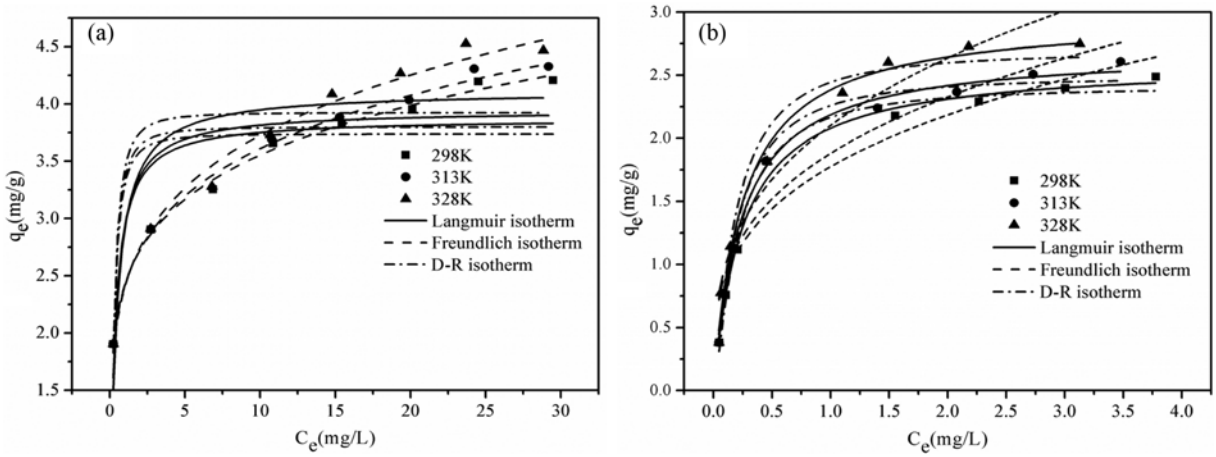

Fig. 5. Equilibrium isotherms of the adsorption of Cr(VI) (a) and As(III) (b).

Table 2. Adsorption isotherm constants for adsorption of Cr(VI) and As(III) by MnO_2/MCM-41

Model	Parameters	Cr(VI)			As(III)		
		298 K	313 K	328 K	298 K	313 K	328 K
Langmuir	q_m (mg/g)	3.872	3.940	4.111	2.601	2.701	2.968
	K_L (L/mg)	3.098	2.900	2.420	3.992	4.254	4.076
	R^2	0.758	0.732	0.699	0.992	0.991	0.988
Freundlich	n	6.020	5.730	5.254	3.334	3.249	3.052
	K_F (mg/g)	2.420	2.410	2.404	1.775	1.880	2.101
	R^2	0.994	0.993	0.985	0.911	0.932	0.932
D-R	q_m (mg/g)	3.707	3.762	3.876	2.350	2.447	2.648
	K (mol^2/kJ^2)	0.004	0.004	0.004	0.003	0.003	0.002
	R^2	0.761	0.739	0.704	0.991	0.980	0.964
	E (kJ/mol)	11.180	11.180	11.180	12.910	12.910	15.811

The adsorption is dominated by chemical ion-exchange if E lies between 8 and 16 kJ/mol, while if E lower than 8 kJ/mol, the adsorption process is of a physical nature [48].

The fitting curves are shown in Fig. 5(a) and Fig. 5(b); the isotherm parameters are all listed in Table 2. Clearly, q_m value increased with increasing temperature. Thus, temperature exhibited positive enhancement on adsorption of both Cr(VI) and As(III). On one hand, the improved temperature provided heavy metal ions with more energy to overcome the rebellion between adsorbent and adsorbate. On the other hand, the number of available active sites on adsorbent surface increased when temperature was increased. The high values of correlation coefficient (R^2>0.985) indicated that Freundlich model was more applicable to the adsorption of Cr(VI) than Langmuir. This results implied that heterogeneous adsorption had occurred on MnO_2/MCM-41 [49]. In addition, the value of 1/n in Freundlich was lower than 1.0 from temperature 298 to 328 K. It meant a heterogeneous surface of MnO_2/MCM-41 [50] and the adsorption by MnO_2/MCM-41 was favorable. As to adsorption of As(III), the Langmuir model fitted the experiment data better. This indicated that As(III) adsorption mainly happened on surface of MnO_2/MCM-41, belonging to monolayer adsorption and there was no mutual effect between the adsorbed ions. E values obtained from Eq. (14) for Cr(VI) and As(III) were all in the range of 8-16 kJ/mol, which suggested that chemical adsorption was involved. Lafferty et al. [51] studied the oxidation of arsenite(III) by Manganese-Oxide and they reported similar chemical process in which arsenite(III) was oxidized into arsenite(V). Parida et al. [25] studied the adsorption of Cr(VI) by TiO_2-MCM-41 and their results were in accordance with ours.

3-3. Kinetic Study

To examine the controlling mechanism of the adsorption process, four kinetic models were used to test the experimental data: pseudo-first-order kinetic model, pseudo-second-order kinetic model, Spahn and Schlunder model and intra-particle diffusion model. The pseudo-first-order kinetic model (Eq. (15)) [52] and pseudo-second-order kinetic model (Eqs. (16) and (17)) [53] are expressed as follows:

$$q_t = q_e\left(1-10^{\frac{-k_1 t}{2.300}}\right) \tag{15}$$

$$\frac{t}{q_t} = \frac{1}{k_2 q_e^2} + \frac{t}{q_e} \tag{16}$$

$$h = k_2(q_e)^2 \tag{17}$$

The nonlinear forms of these two models are illustrated in Fig. 6. The kinetic parameters with correlation coefficients are tabulated in Table 3. Higher R^2 values showed that the kinetic data obtained

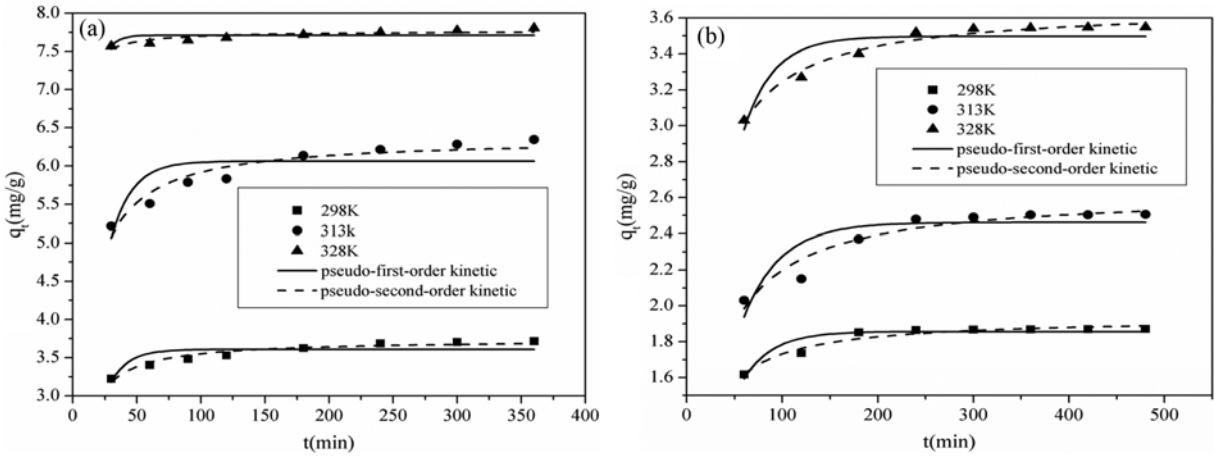

Fig. 6. The pseudo-first-order and pseudo-second-order kinetic of Cr(VI) (a) and As(III) (b).

Table 3. Pseudo-first-order, pseudo-second-order, Spahn and Schlunderl and intra-particle diffusion model kinetic parameters for Cr(VI) and As(III) adsorption by MnO_2/MCM-41

Ion	Ion concentration (mg/L)	Pseudo-first-order			Pseudo-second-order			Spahn and Schlunder		Intra-particle diffusion model			
		k_1	q_e (mg/g)	R^2	h (mg/g·min)	q_e (mg/g)	R^2	k_{ext} (min^{-1})	R^2	$k_{p,2}$	R^2	$k_{p,3}$	R^2
Cr(VI)	10	0.1643	3.607	0.5888	0.7109	3.738	0.9381	−0.00243	0.9979	0.226	0.9723	0.213	0.9960
	20	0.1382	6.064	0.5454	0.8122	6.372	0.9085	−0.00142	0.9999	0.420	0.9846	0.366	0.9980
	30	0.3056	7.712	0.2582	8.1645	7.771	0.9796	−0.00014	0.9236	0.082	0.9429	0.162	0.9966
As(III)	2	0.0750	1.857	0.8422	0.1498	1.936	0.9430	−0.00352	0.9889	0.441	0.9994	0.178	0.9853
	5	0.0594	2.461	0.7127	1.3092	2.625	0.9145	−0.00260	0.9687	0.624	0.9916	0.307	0.9989
	8	0.0732	3.497	0.7731	2.2688	3.666	0.9263	−0.00223	0.9681	0.811	0.9969	0.446	0.9984

from experiment results fitted well to pseudo-second-order kinetic model, so chemical adsorption controlled the rate of the adsorption process. In addition, Table 3 shows that h value increased along with increase of initial metal concentration from 0.7109 to 8.1645 and 0.1498 to 2.2688 for Cr(VI) and As(III), respectively. This result gave the idea that increase of initial metal concentration led to increased metal ion diffusion rate; thus the collision chance of metal ions with adsorbent increased, promoting the adsorption process. Moreover, as can be seen from Table 3, both the q_e value of Cr(VI) and As(III) increased, accompanied with the increase of metal concentration.

The Spahn and Schlunder model [54] was chosen to analyze external diffusion, that is, metal ions diffuse from solution to adsorbent surface:

$$\ln C_t = \ln C_0 - k_{ext} t \quad (18)$$

If external diffusion rate is dominant in the whole adsorption process, $\ln C_t$ should have a good linear relationship with t. Fig. 7(a) and Fig. 7(b) show plots of $\ln C_t$ versus t for Cr(VI) and As(III) adsorption at different initial concentrations, respectively. The parameters of Spahn and Schlunder model are also listed in Table 3. From Fig. 7(a) and Fig. 7(b), there exists good linearity in the initial 250 min, which means external diffusion was the rate-controlling step in the initial adsorption stage. In addition, the abstract value of k_{ext} decreased along with the increase of initial Cr(VI) concentration. This may be attributed to the bigger repulsive force between metal ions at high initial concentration; therefore the diffusion rate decreased.

The intra-particle diffusion model [55] is always used to describe ion diffusion in the micropore of adsorbent:

$$q_t = k_{p,i} t^{0.5} + C \quad (19)$$

In terms of this model, if the plot of q_t versus $t^{0.5}$ gives a straight line, then intra-particle diffusion is involved in the adsorption process; and if this line passes through the origin, then intra-particle diffusion is the rate-controlling step [56]. Whereas, if the data present multi-linear plots, then two or more steps influence the adsorption process, such as external diffusion, intra-particle diffusion and so on [57,58]. The plot of q_t versus $t^{0.5}$ is presented in Fig. 8. Multi-linearity of the plots indicated that two more steps occurred during the adsorption processes. The first portion was by the external diffusion, metal ions diffuse from solution to adsorbent surface; following portion corresponding to intra-particle diffusion, metal ions diffuse into the internal pores and are adsorbed by inner active sites.

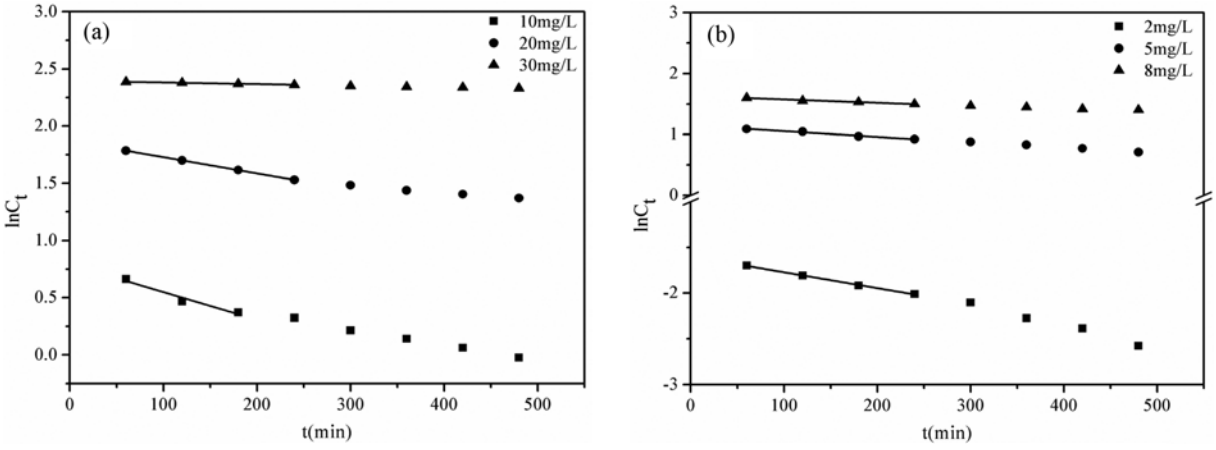

Fig. 7. Spahn and Schlunder model for the adsorption of Cr(VI) (a) and As(III) (b) by MnO_2/MCM-41.

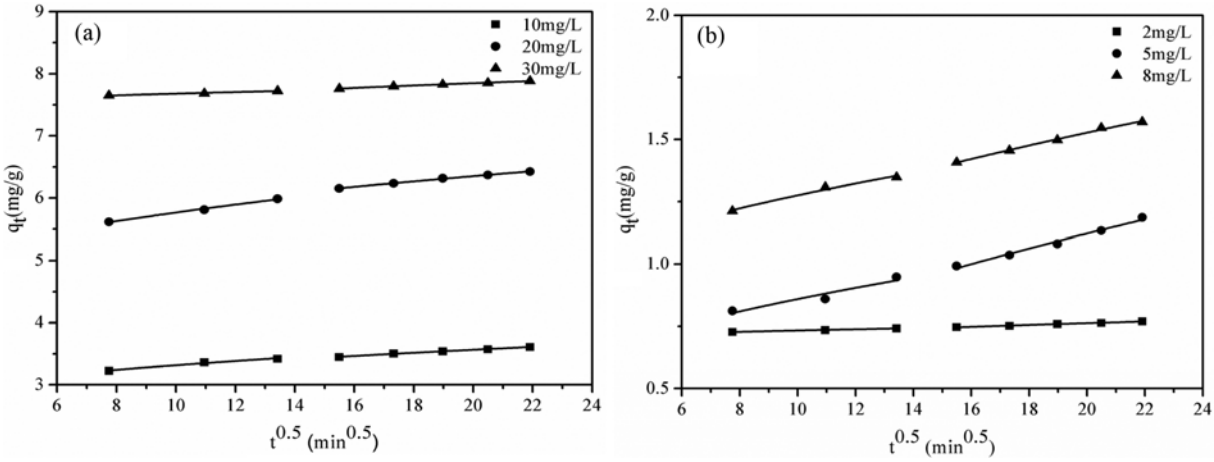

Fig. 8. Intra-particle diffusion model for the adsorption of Cr(VI) (a) and As(III) (b) by MnO_2/MCM-41.

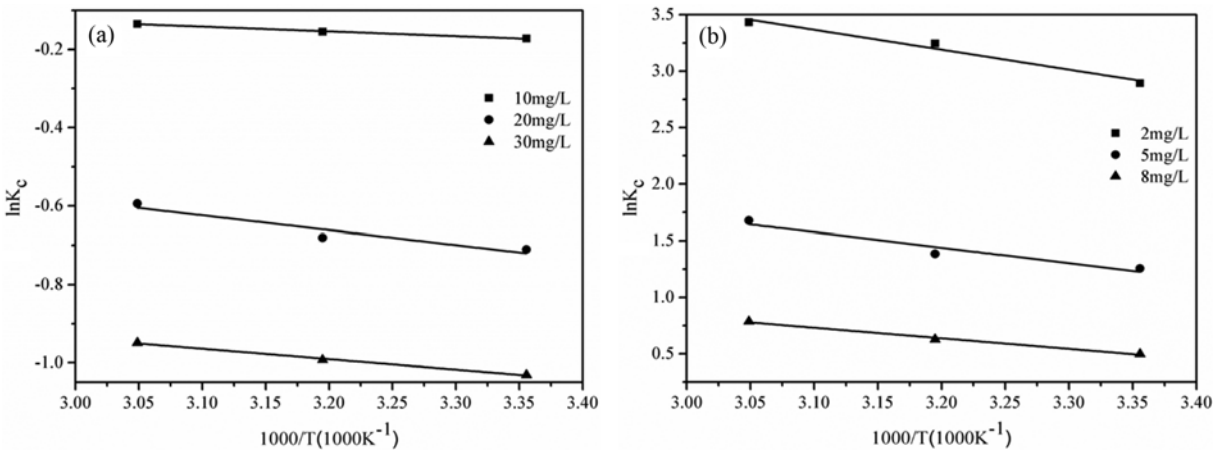

Fig. 9. Van't Hoff plot for the adsorption of Cr(VI) (a) and As(III) (b) by MnO_2/MCM-41.

Table 4. Thermodynamic parameters for adsorption of Cr(VI) and As(III) on MnO_2/MCM-41

Ion	C_0 (mg/L)	ΔH^0 (kJmol^{-1})	ΔS^0 (kJmol^{-1}K^{-1})	ΔG^0 (kJmol^{-1})				
				293 K	298 K	303 K	308 K	313 K
Cr(VI)	10	1.020	1.985	−40.621	−46.286	−51.099	−54.198	−58.656
	20	0.731	1.520	−28.414	−30.524	−31.276	−33.671	−40.804
	30	0.224	1.120	−17.804	−20.992	−21.796	−24.026	−26.714
As(III)	2	14.713	73.608	−16.77	−18.249	−20.970	−26.825	−32.044
	5	11.346	48.269	−8.4890	−11.386	−12.734	−15.360	−25.389
	8	7.788	30.225	−2.4685	−3.7233	−8.9411	−16.416	−18.135

Values of $k_{p,2}$, $k_{p,3}$ and correlation coefficients are given in Table 3.

3-4. Thermodynamic Study

In this part, the change in free energy (ΔG^0), enthalpy (ΔH^0) and entropy (ΔS^0) was calculated from equations as follows:

$$K_0 = \frac{C_{ad}}{C_e} \tag{20}$$

$$\Delta G = -RT \ln K_0 \tag{21}$$

$$\ln K_0 = \frac{\Delta S^o}{R} - \frac{\Delta H^o}{RT} \tag{22}$$

Fig. 9(a) and Fig. 9(b) show the van't Hoff plot of $\ln k_0$ versus 1000/T, ΔH^0 and ΔS^0 could be obtained from the slope and intercept, respectively.

The thermodynamic parameters are summarized in Table 4. Negative values of ΔG^0 indicate the feasible and spontaneous nature of the sorption process. Positive ΔH^0 values suggest that the adsorption process was endothermic, and positive ΔS^0 showed the affinity of MnO_2/MCM-41 for Cr(VI) and As(III) ions.

4. Adsorption Tests in Binary System

4-1. Effect of pH

Fig. 10 shows the effect of pH on the adsorption of Cr(VI) at the presence of As(III) in pH range of 2-9. Below pH 5, there was no pronounced inhibitory effect on Cr(VI) adsorption in the presence of As(III). At pH of 2-5, the positively charged adsorbent had strong affinity to Cr(VI) ions ($HCrO_4^-$ and CrO_4^{2-}), while uncharged As(III) (H_3AsO_3) could not compete with Cr(VI) ions for adsorption sites [59]. Above pH 5, As(III) exerted a inhibitory effect on Cr(VI) adsorption. This may due to the competition between negatively charged As(III) ($H_2AsO_4^-$) and Cr(VI) ($HCrO_4^-$ or CrO_4^{2-}) [60]. Adsorption of As(III) was slightly reduced in the presence of Cr(VI), as illustrated in Fig. 10, which means that Cr(VI) restrained the adsorption of As(III). The most likely reason for this antagonistic effect was that Cr(VI) was prior to be adsorbed by MnO_2/MCM-41. Moreover, the adsorption behavior was complex in binary component system. And several factors were deemed to be rela-

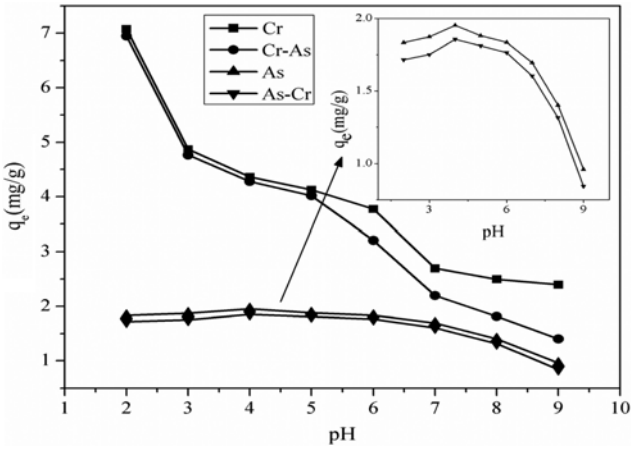

Fig. 10. Effect of pH on the removal of Cr(VI) and As(III) from binary system.

Table 5. Kinetic parameters for adsorption of Cr(VI) and As(III) in binary system

Ion	Coexist ion concentration (mg/L)	Pseudo-first-order kinetic			Pseudo-second-order kinetic		
		k_1 (min^{-1})	q_e (mg/g)	R^2	k_2 (g/(mg min)	q_e (mg/g)	R^2
Cr(VI)	C_{As}=5	0.1440	2.589	0.4791	0.1678	2.614	0.9383
	C_{As}=10	0.1435	2.559	0.4397	0.1677	2.584	0.9384
	C_{As}=20	0.1429	2.519	0.4795	0.1676	2.544	0.9385
As(III)	C_{Cr}=5	0.0980	2.147	0.4828	0.0901	2.126	0.9397
	C_{Cr}=10	0.1369	2.169	0.4824	0.1662	2.194	0.9395
	C_{Cr}=20	0.1374	2.199	0.4821	0.1664	2.224	0.9394

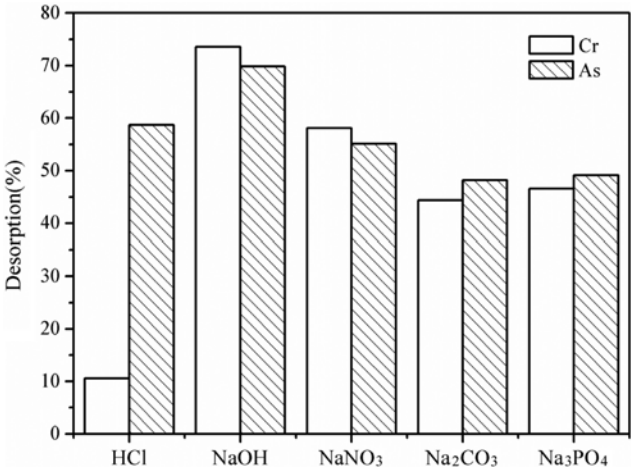

Fig. 11. The effect of different desorption reagents on the desorption of metal ions-loaded MnO_2/MCM-41.

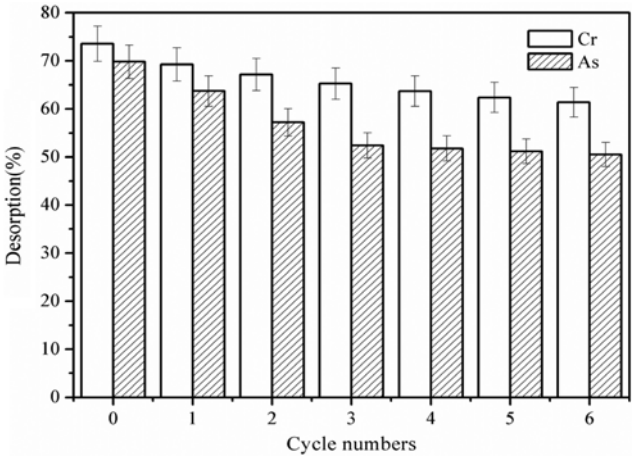

Fig. 12. Reusability of MnO_2/MCM-41 with repeated sorption-desorption cycles.

tional, such as, electrostatic attraction due to charge to radius ratio and adsorption sites are suitable for one metal ion over another [61].

4-2. Binary System Adsorption Kinetics

The pseudo-first-order kinetic and pseudo-second-order kinetic models were also applied to study the adsorption kinetics of Cr(VI) and As(III) in a binary system. Related kinetic parameters and coefficient correlation are shown in Table 5, where it is seen that that the pseudo-second-order kinetic model still fitted well to the adsorption data. Adsorption capacity of Cr(VI) decreased along with the increase of coexist As(III) concentration. Moreover, the adsorption rate of Cr(VI) decreased accompanied by the increased As(III) concentration.

5. Desorption and Reusability of Adsorbent

Desorption is a significant component of adsorption studies to reuse adsorbent. So in order to make MnO_2/MCM-41 more usable in real work, several experiments were done to select the effective desorption reagents. As shown in Fig. 11, NaOH was the most effective reagent among the five kinds of desorption reagents. The highest desorption efficiency was 73.54% for Cr(VI) and 69.81% for As(III). In addition, $NaNO_3$ and HCl also exhibited quite good effect on desorption of Cr(VI)-loaded and As(III)-loaded MnO_2/MCM-41, respectively. Fig. 12 shows that the adsorption ability of MnO_2/MCM-41 decreased with increase of recycle times. After six times of recycle, the removal efficiency decreased by 12.14% and 19.3% for Cr(VI) and As(III), respectively, with HCl as desorption reagent. The result demonstrated that MnO_2/MCM-41 has a high value for reuse.

CONCLUSIONS

MnO_2/MCM-41, geared up by synthesis, turned out to be an efficient adsorbent for Cr(VI) and As(III) adsorption in single and binary system. The XRD, XRF and SEM analysis demonstrated that MnO_2 was successfully loaded on MCM-41, and the structure of MCM-41 was retained after loading of MnO_2. pH dramatically affected the adsorption processes of Cr(VI) and As(III). It can be concluded that the highest adsorption capacity of 0.5 g MnO_2/MCM-41 for Cr(VI) takes place at pH 2, 328 K and initial Cr(VI) concentration of 30 mg/L; for As(III) at pH 4, 328 K and initial As(III) concentration of 8 mg/L. The equilibrium adsorption data of Cr(VI) fitted better to Freundlich model in mono-component system, indicating heterogeneous adsorption reaction happened on MnO_2/MCM-41. Whereas, the suitability of Langmuir for As(III) adsorption meant that As(III) adsorption mainly occurred on the surface of the adsorbent. In addition, the adsorption of Cr(VI) and As(III) on MnO_2/MCM-41 followed pseudo-second-order kinetic with external diffusion and intra-particle diffusion controlling the adsorption rate. The obtained thermodynamic parameters revealed the feasibility, endothermic and spontaneous property of the adsorption process. In a binary system, the presence of As(III) inhibited the removal of Cr(VI) only when pH was greater than 5.0, While,

Cr(VI) exhibited a restraint on As(III) removal at pH 2-9. Furthermore, the MnO_2/MCM-41 showed good reusability.

NOMENCLATURE

C_0 : initial liquid concentration of metal ions [mg/L]
C_2 : the final liquid concentration of metal ions after desorption [mg/L]
C_{ad} : metal concentration at adsorbate phase [mg/L]
C_e : liquid phase metal ion concentration at equilibrium [mg/L]
C_t : liquid concentration of metal ions at time t [mg/L]
E : mean free energy [kJ/mol]
H : initial adsorption rate [mg/g·min]
K_0 : equilibrium constant [L/g]
k_1 : equilibrium rate constant of pseudo-first-order sorption [min^{-1}]
k_2 : equilibrium rate constant of pseudo-first-order sorption [g/(mg min)
K_{DR} : activity coefficient related to adsorption mean free energy [mol^2/kJ^2]
k_{ext} : external diffusion rate constant [1/min]
K_F : Freundlich constant indicative of the relative sorption capacity of the sorbent [mg/g]
K_L : Langmuir adsorption constant [L/mg]
$k_{p,I}$: intra-particle diffusion rate constant at different stages
K : ionization equilibrium constant
M : the mass of dry adsorbent [g]
n : Freundlich constant indicative of the intensity of sorption
q_e : the adsorption capacity of at equilibrium [mg/g]
q_m : maximum sorption capacity of adsorbent [mg/g]
q_t : amount of metal ions adsorbed per unit weight of adsorbent at time t [mg/g]
R : gas constant [8.314 J/mol/K]
T : solution temperature [K]
V_1 : volume of solution in adsorption experiment [mL]
V_2 : volume of solution in desorption experiment [mL]
V : the solution volume [mL]
β : the desorption efficiency [%]
ε : polanyi potential

REFERENCES

1. F. Fu and Q. Wang, *J. Environ. Manage.*, **92**, 407 (2011).
2. G. Bayramoglu and M. Yakuparica, *Chem. Eng. J.*, **139**, 20 (2008).
3. C. E. Barrera-Díaz, V. Lugo-Lugo and B. Bilyeu, *J. Hazard. Mater.*, **223**, 1 (2012).
4. C. A. Kozlowski and W. Walkowiak, *Water Res.*, **36**, 4870 (2002).
5. J. Saiz, E. Bringas and I. Ortiz, *J. Chem. Technol. Biotechnol.*, **89**, 909 (2014).
6. V. M. Boddu, K. Abburi, J. L. Talbott, E. D. Smith and R. Haasch, *Water Res.*, **42**, 633 (2008).
7. B. K. Mandal and K. T. Suzuki, *Talanta*, **58**, 201 (2002).
8. Y. Salameh, N. Al-Lagtah, M. Ahmad, S. Allen and G. Walker, *Chem. Eng. J.*, **160**, 440 (2010).
9. M. Owlad, M. K. Aroua, W. A. W. Daud and S. Baroutian, *Water, Air, Soil Pollut.*, **200**, 59 (2009).
10. D. Mohan and C. U. Pittman Jr., *J. Hazard. Mater.*, **142**, 1 (2007).
11. M. Rafatullah, O. Sulaiman, R. Hashim and A. Ahmad, *J. Hazard. Mater.*, **170**, 969 (2009).
12. A. K. Giri, R. Patel and S. Mandal, *Chem. Eng. J.*, **185**, 71 (2012).
13. A. E. Nemr, *J. Hazard. Mater.*, **161**, 132 (2009).
14. M. Aryal and M. Liakopoulou Kyriakides, *J. Chem. Technol. Biotechnol.*, **89**, 559 (2014).
15. R. Muzzarelli and R. Rocchetti, *Trace Metal Removal from Aqueous Solution*, The Royal Society of Chemistry, London (1986).
16. R. L. Chaney and P. T. Hundemann, *J. Water Pollut. Control Fed.*, **51**, 17 (1979).
17. A. B. Albadarin, C. Mangwandi, A. a. H. Al-Muhtaseb, G. M. Walker, S. J. Allen and M. N. Ahmad, *Chem. Eng. J.*, **179**, 193 (2012).
18. J. Hizal and R. Apak, *J. Colloid Interface Sci.*, **295**, 1 (2006).
19. L. Niu, S. Deng, G. Yu and J. Huang, *Chem. Eng. J.*, **165**, 751 (2010).
20. M. R. Samani, S. M. Borghei, A. Olad and M. J. Chaichi, *J. Hazard. Mater.*, **184**, 248 (2010).
21. M. R. Mello, D. Phanon, G. Q. Silveira, P. L. Llewellyn and C. M. Ronconi, *Micropor. Mesopor. Mater.*, **143**, 174 (2011).
22. P. A. Mangrulkar, S. P. Kamble, J. Meshram and S. S. Rayalu, *J. Hazard. Mater.*, **160**, 414 (2008).
23. H. Yang, R. Xu, X. Xue, F. Li and G. Li, *J. Hazard. Mater.*, **152**, 690 (2008).
24. J. Cao, Y. Wu, Y. Jin, P. Yilihan and W. Huang, *J. Taiwan Inst. Chem. Eng.*, **45**, 860 (2014).
25. K. Parida, K. G. Mishra and S. K. Dash, *J. Hazard. Mater.*, **241**, 395 (2012).
26. E. Hu and H. Cheng, *Water Res.*, **57**, 8 (2014).
27. J. Ge and J. Qu, *J. Hazard. Mater.*, **100**, 197 (2003).
28. H. Jin, J. Yuan, H. Hao, Z. Ji, M. Liu and S. Hou, *Mater. Lett.*, **110**, 69 (2013).
29. S. G. Wang, W. X. Gong, X. W. Liu, Y. W. Yao, B. Y. Gao and Q. Y. Yue, *Sep. Purif. Technol.*, **58**, 17 (2007).
30. L. Dong, Z. Zhu, H. Ma, Y. Qiu and J. Zhao, *J. Environ. Sci.*, **22**, 225 (2010).
31. S. K. Jana, H. Takahashi, M. Nakamura, M. Kaneko, R. Nishida, H. Shimizu, T. Kugita and S. Namba, *Appl. Catal. A*, **245**, 33 (2003).
32. B. Han, F. Zhang, Z. Feng, S. Liu, S. Deng, Y. Wang and Y. Wang, *Ceram. Int.*, **40**, 8093 (2014).
33. X. Song, P. Qu, N. Jiang, H. Yang and G. Qiu, *Colloids Surf., A: Physicochem. Eng. Asp.*, **313**, 193 (2008).
34. N. A. Fathy, S. E. El-Shafey, O. I. El-Shafey and W. S. Mohamed, *J. Environ. Chem. Eng.*, **1**, 858 (2013).
35. M. Szlachta, V. Gerda and N. Chubar, *J. Colloid Interface Sci.*, **365**, 213 (2012).
36. X. Xie and L. Gao, *Carbon*, **45**, 2365 (2007).
37. Y. S. Ding, X. F. Shen, S. Gomez, H. Luo, M. Aindow and S. L. Suib, *Adv. Funct. Mater.*, **16**, 549 (2006).
38. R. I. Kureshy, I. Ahmad, N. u. H. Khan, S. H. Abdi, K. Pathak and R. V. Jasra, *J. Catal.*, **238**, 134 (2006).
39. Y. Salameh, N. Al-Lagtah, M. N. M. Ahmad, S. J. Allen and G. M. Walker, *Chem. Eng. J.*, **160**, 440 (2010).
40. D. Mohan, K. P. Singh and V. K. Singh, *Ind. Eng. Chem. Res.*, **44**, 1027 (2005).
41. S. K. Prabhakaran, K. Vijayaraghavan and R. Balasubramanian, *Ind. Eng. Chem. Res.*, **48**, 2113 (2009).

42. A. S. K. Kumar, S. Kalidhasan, V. Rajesh and N. Rajesh, *Ind. Eng. Chem. Res.*, **51**, 58 (2011).
43. Y. Wu, Y. Wen, J. Zhou, J. Cao, Y. Jin and Y. Wu, *Environ. Sci. Pollut. R.*, **20**, 2210 (2013).
44. H. Nesbitt, I. Muir and A. Prarr, *Geochim. Cosmochim. Acta*, **59**, 1773 (1995).
45. I. Langmuir, *J. Am. Chem. Soc.*, **40**, 1361 (1918).
46. H. Freundlich, *Z. Physik. Chem.*, **57**, 385 (1907).
47. A. Sari, M. Tuzen, D. Citak and M. Soylak, *J. Hazard. Mater.*, **149**, 283 (2007).
48. M. S. Onyango, Y. Kojima, A. Kumar, D. Kuchar, M. Kubota and H. Matsuda, *Sep. Sci. Technol.*, **41**, 683 (2006).
49. C. Özeroğlu, E. Doğan and G. Keçeli, *J. Radioanal. Nucl. Chem.*, **289**, 577 (2011).
50. S. Bagherifam, A. Lakzian, S. J. Ahmadi, M. F. Rahimi and A. Halajnia, *J. Radioanal. Nucl. Chem.*, **283**, 289 (2010).
51. B. J. Lafferty, M. Ginder-Vogel and D. L. Sparks, *Environ. Sci. Technol.*, **44**, 8460 (2010).
52. H. S. Hassan, M. F. Attallah and S. M. Yakout, *J. Radioanal. Nucl. Chem.*, **286**, 17 (2010).
53. Y. S. Ho and G. McKay, *Water Res.*, **34**, 735 (2000).
54. W. Fritz, W. Merk and E. Schluender, *Chem. Eng. Sci.*, **36**, 743 (1981).
55. Y. S. Ho and G. McKay, *Process Saf. Environ. Prot.*, **76**, 183 (1998).
56. J. P. Chen, S. Wu and K. H. Chong, *Carbon*, **41**, 1979 (2003).
57. F. N. Behdani, A. T. Rafsanjani, M. Torab-Mostaedi and S. M. A. K. Mohammadpour, *Korean J. Chem. Eng.*, **30**, 448 (2013).
58. H. Wang, N. Yan, Y. Li, X. Zhou, J. Chen, B. Yu, M. Gong and Q. Chen, *J. Mater. Chem.*, **22**, 9230 (2012).
59. Y. Wu, J. Zhou, Y. Jin, J. Cao, P. Yilihan, Y. Wen and Y. Wu, *Environ. Sci. Pollut. R.*, **21**, 1859 (2014).
60. P. X. Sheng, Y. P. Ting and J. P. Chen, *Ind. Eng. Chem. Res.*, **46**, 2438 (2007).
61. A. Roy and J. Bhattacharya, *Sep. Purif. Technol.*, **115**, 172 (2013).